

Quasielastic Scattering from Relativistic Bound Nucleons: Transverse-Longitudinal Response

J.M. Udias^{1,a}, J.A. Caballero^{1,b}, E. Moya de Guerra¹, J.E. Amaro² and T.W. Donnelly³

¹Instituto de Estructura de la Materia, CSIC Serrano 123, Madrid, Spain

^aDepartamento de Física Atómica, Molecular y Nuclear, Universidad Complutense de Madrid, Madrid, Spain

^bDepartamento de Física Atómica, Molecular y Nuclear, Universidad de Sevilla, Apdo. 1065, Sevilla, Spain

²Departamento de Física Moderna, Universidad de Granada, Granada, Spain

³Center for Theoretical Physics, Laboratory for Nuclear Science and Department of Physics, Massachusetts Institute of Technology, Cambridge, USA

Abstract

Predictions for electron induced proton knockout from the $p_{1/2}$ and $p_{3/2}$ shells in ^{16}O are presented using various approximations for the relativistic nucleonic current. Results for the differential cross section, transverse-longitudinal response (R_{TL}) and left-right asymmetry A_{TL} are compared at $|Q^2| = 0.8$ $(\text{GeV}/c)^2$ corresponding to TJNAF experiment 89-003. We show that there are important dynamical and kinematical relativistic effects which can be tested by experiment.

PACS: 25.30.Fj; 25.30.Rw; 24.10.-i; 21.60.Cs

Keywords: Quasielastic electron scattering; Negative-energy components; Transverse-longitudinal response; Left-right asymmetry.

Under quasielastic conditions the $(e, e'p)$ reaction can be treated with confidence [1] via the impulse approximation in which the detected proton absorbs the entire momentum (\vec{q}) and energy (ω) lost by the electron. Detecting the outgoing proton in coincidence with the scattered electron allows one to determine the missing energy (E_m) and momentum (p_m) in the reaction and thus to provide detailed information on the energies, momentum distributions and spectroscopic factors of bound nucleons [1,2]. Until recently low- E_m data were concentrated at $p_m \leq 300$ MeV/c. Now higher p_m -regions are being probed at small E_m under quasielastic conditions [3,4], yielding new information in a regime where two-body currents (meson exchange currents and Δ -isobar contributions) can be safely neglected [5,6].

Most theoretical work on $(e, e'p)$ has been carried out on the basis of nonrelativistic approximations to the nucleon current. Specifically, the standard distorted wave impulse approximation (DWIA) [1] has been extensively employed [2] to analyze $(e, e'p)$ data, using nonrelativistic current operators with bound and scattered proton wave functions deduced from phenomenological nonrelativistic potentials. However, DWIA analyses have met two major difficulties: a) The spectroscopic factors extracted from low- p_m data are too small compared with theoretical predictions [7]. For instance, the extracted occupations of $3s_{1/2}$ and $2d_{5/2}$ orbits in ^{208}Pb are $S_\alpha \simeq 0.5$, while theories on short-range correlations [7] predict at most a 30% reduction of mean-field occupations for levels just below the Fermi level. b) DWIA calculations compatible with the low- p_m data predict much smaller cross sections at high- p_m than those experimentally observed [3]. Although short-range correlations are expected to increase the high-momentum components, their effect is negligible [8] at the small missing energies of these high- p_m data, and effects of long-range correlations have been invoked [3].

In recent years the relativistic mean-field approximation has been successfully used for the analyses of both low- p_m [9–13] and high- p_m [14] data. In the relativistic distorted-wave impulse approximation (RDWIA), the nucleon current

$$J_N^\mu(\omega, \vec{q}) = \int d\vec{p} \bar{\psi}_F(\vec{p} + \vec{q}) \hat{J}_N^\mu(\omega, \vec{q}) \psi_B(\vec{p}) \quad (1)$$

is calculated with relativistic ψ_B and ψ_F wave functions for initial bound and final outgoing nucleons, respectively. \hat{J}_N^μ is the relativistic nucleon current operator of $cc1$ or $cc2$ forms as in [15]. The bound state wave function is a four-spinor with well-defined parity and angular momentum quantum numbers and is obtained by solving the Dirac equation with scalar-vector (S-V) potentials determined through a Hartree procedure from a relativistic Lagrangian with scalar and vector meson terms [16]. The wave function for the outgoing proton is a solution of the Dirac equation containing S-V global optical potentials [17] for a nucleon scattered with asymptotic momentum \vec{p}_F . In contrast to DWIA, in RDWIA the analyses of individual nuclear shells were done with no fitting parameters other than the spectroscopic factors [10–13]. The RDWIA spectroscopic factors obtained are larger than the DWIA ones [11–13] and are valid both for low- and high- p_m data [14] — for the above-mentioned $3s_{1/2}$ and $2d_{3/2}$ shells in ^{208}Pb , values of $S_\alpha \simeq 0.7$ have been obtained [11,13] together with reasonable agreement at high- p_m [14].

We have recently studied [18,19] the effect on the individual response functions of the relativistic treatment of the nucleon current. Focussed on the relativistic plane wave impulse approximation (RPWIA) we showed [18] that the TL response is very sensitive to the negative-energy components of the relativistic bound nucleon wave function. We have also

shown [19] that, for the $j = l \pm 1/2$ spin-orbit partners of a given shell, this sensitivity is much larger for the $j = l - 1/2$ than for the $j = l + 1/2$ case. Strong sensitivity of the TL response to relativistic corrections was earlier found for $d(e, e'p)$ [20].

A certain degree of controversy surrounds the TL response measured in exclusive quasielastic electron scattering from the least bound protons in several nuclei (^{12}C , ^{16}O , ^{208}Pb): in some cases [21] large deviations from standard DWIA calculations appear, while in others [9] the data are close to the calculations. New data on the R_{TL} response for proton knockout from the $1p_{1/2}$ and $1p_{3/2}$ orbits of ^{16}O are expected soon from an experiment carried out at Jefferson Laboratory (TJNAF) [22] at $|Q^2| \cong 0.8$ (GeV/c) 2 and perpendicular kinematics. The purpose of this Letter is to show for this case that there are important kinematical and dynamical relativistic effects.

For the bound state wave functions we use the parameters of the set NLSH in [23]. We have also obtained results with the older HS set [16,24], as well as with the newest NL3 one [25], and found very similar results. For the scattered proton wave function, we use the energy-dependent, A -independent, potentials derived by Clark *et al.* [17] for ^{16}O . Again, we checked that using other relativistic optical potentials does not alter our results and conclusions. The kinematical conditions follow closely those of the TJNAF proposal [22]: beam energy 2445 MeV, $|\vec{q}| \simeq 1$ GeV/c, $\omega \simeq 439$ MeV, corresponding to quasielastic kinematics ($\omega \simeq |Q^2|/2/M$), and proton kinetic energy of about 427 MeV; the angle θ_F of the outgoing proton with respect to \vec{q} is varied and thus the missing momentum varies as $p_m^2 = |\vec{q}|^2 + |\vec{p}_F|^2 - 2|\vec{p}_F||\vec{q}| \cos \theta_F$.

Figure 1 shows the differential cross section, R_{TL} response and TL asymmetry (A_{TL}) for $p_{1/2}$ (top panels) and $p_{3/2}$ (bottom panels). R_{TL} and A_{TL} are obtained from the cross sections measured at $\phi_F = 0^\circ$ and $\phi_F = 180^\circ$ with the other variables (ω, Q^2, E_m, p_m) held constant, where ϕ_F is the azimuthal angle of the scattered proton (we follow the same convention as in [22]). Relativistic calculations using the *cc1* and *cc2* current operators are shown by solid and dotted lines, respectively. The Coulomb gauge has been used throughout and we have checked that, as in our previous work (see in particular [18]), the Landau and Coulomb gauges produce similar results. On the contrary, the Weyl gauge produces important deviations (larger for $p_{1/2}$ and *cc1*) and tends to give unrealistic enhancements of the longitudinal current [18]. We use a spectroscopic factor $S_\alpha = 0.7$ as obtained for ^{208}Pb [11], which in RDWIA also matches the low- p_m data [9,26] for the shells discussed here; the spectroscopic factor simply scales down the curves for differential cross sections and R_{TL} while leaving A_{TL} unchanged.

We can divide the differences between this fully relativistic approach and the standard nonrelativistic one into two categories: *i*) Effects due to the fully relativistic current operator, *i.e.*, 4×4 matrix structure of the 4-vector current operator, compared to the 2×2 matrix structure of the nonrelativistic current operator which is usually expanded in \vec{p}/M . We call these effects *kinematical* as they are in principle independent of the dynamics introduced by the nuclear interaction. *ii*) Effects due to the differences between relativistic and non-relativistic nucleon wave functions, which of course depend not only on the 4-spinor versus 2-spinor structure, but also on the potentials used in the respective Dirac and Schrödinger equations. Thus we call these effects *dynamical*.

Further insight into these differences can be gained recalling the steps taken in nonrelativistic approaches. First, the one-body current operator is expanded in a basis of free-

nucleon plane-waves, which amounts to a truncation of the nucleon propagator that ignores negative-energy solutions of the free Dirac equation. This is common to PWIA and DWIA. Second, to take into account (spin-dependent) final-state interactions or distortion effects, in DWIA the current operator is transformed into a 2×2 matrix (usually involving \vec{p}/M expansions) to calculate the nucleon current as the matrix element between the nonrelativistic bound (χ_B) and scattered (χ_F) wave functions. This second step is not needed in PWIA, which can then better incorporate the relativistic kinematics, but misses important absorption effects. A “relativized” form of the 2×2 current operator was proposed in [27,28] to optimize the \vec{p}/M expansion.

One may then identify two types of relativistic dynamical effects:

ii – a) Dynamical effects coming from the difference between the upper components of ψ_F (ψ_B) and the solutions χ_F (χ_B) of the Schrödinger equation. Assuming equivalent central and spin-orbit potentials, this difference stems from the well-known Darwin term. Provided that the relativistic dynamics are known, one can deduce the Darwin term and construct an equivalent bi-spinor wave function χ to include its effect in the nonrelativistic nucleon current, thus removing this source of difference between relativistic and nonrelativistic results [12]. This is done for instance in ref. [29]. The influence of this term on $(e, e'p)$ observables has been demonstrated in several works [11,12,30,31]. It appears to be the main dynamical relativistic effect in the cross section in the low- p_m region [11,12], and is important for the correct determination of the spectroscopic factor from low- p_m data. Its omission reduces the spectroscopic factor by 15–20%. It is included in all calculations presented here.

ii – b) The other dynamical effect is due to the negative-energy components of the relativistic ψ_B , ψ_F wave functions. Starting from Schrödinger-like solutions χ one may at best construct properly normalized four-spinors of the form

$$\psi = \frac{1}{\sqrt{N}} \left(\chi(\vec{p}), \frac{\vec{\sigma} \cdot \vec{p}}{E + M} \chi(\vec{p}) \right) \quad (2)$$

to calculate the relativistic nucleon current. However, this spinor lacks the dynamical enhancement of the lower component of the Dirac solution due to the relativistic S-V potentials. This dynamical enhancement is contained in the negative-energy components of the relativistic ψ_B (ψ_F) solutions and influences $(e, e'p)$ observables in the high- p_m regions [12,18]. A discussion of how this effect may be incorporated in nonrelativistic formulations based on 2×2 matrix, \vec{p}/M expansions of current operators modified to include the effects of the relativistic S-V potentials can be found in [32].

The role of the negative-energy components can be seen in Fig. 1 comparing the solid with the short-dashed lines. The dashed lines show the results obtained with the *cc1* current operator when the negative-energy components are projected out, *i.e.*, the nucleon current is calculated as

$$J_{N(++)}^\mu(\omega, \vec{q}) = \int d\vec{p} \bar{\psi}_F^{(+)}(\vec{p} + \vec{q}) \hat{J}^\mu(\omega, \vec{q}) \psi_B^{(+)}(\vec{p}), \quad (3)$$

where $\psi_B^{(+)}$ ($\psi_F^{(+)}$) is the positive-energy component of ψ_B (ψ_F), *i.e.*,

$$\psi_B^{(+)}(\vec{p}) = \Lambda_{(+)}(\vec{p}) \psi_B(\vec{p}), \quad \Lambda_{(+)}(\vec{p}) = \frac{M + \vec{p}}{2M}, \quad (4)$$

with $\bar{p}_\mu = (\bar{E}, \vec{p})$ and $\bar{E} = \sqrt{\vec{p}^2 + M^2}$ (similarly for $\psi_F^{(+)}$). The difference between the solid and short dashed lines is due to the dynamical enhancement of the lower components which is contained in the current of eq. (1), but not in eq. (3). This effect is more visible than that introduced by the theoretical uncertainty due to the choice of $cc1$ (solid line) or $cc2$ (dotted line) operators. It is important to realize that the positive-energy projectors inserted in eq. (3) depend on the integration variable \vec{p} . One may attempt to neglect this dependence by using projection operators corresponding to asymptotic values of the momenta, *i.e.* projectors acting on ψ_F and ψ_B respectively, with $P_F^\mu = (E_F, \vec{p}_F)$, $P_F^\mu - \bar{Q}^\mu$ the asymptotic four-momentum of the outgoing and bound nucleon respectively, with $\bar{Q}_\mu = (\bar{\omega}, \vec{q})$ and $\bar{\omega} = E_F - \sqrt{(\vec{p}_F - \vec{q})^2 + M^2}$. We refer to this approach as *asymptotic projection*. The results corresponding to this approximation are shown by long dashed lines in Fig. 1. They are obtained with the $cc1$ operator and are very similar for $cc2$.

The differential cross sections for $|p_m| < 300$ MeV/c are similar, but show a substantial dependence on the negative-energy components for $|p_m| > 300$ MeV/c for either the $p_{1/2}$ or $p_{3/2}$ shells. Note also that the cross sections obtained with positive-energy projected wave functions are more symmetrical around $p_m = 0$ than the RDWIA results. Therefore, the effect of removing the negative-energy components shows up more in R_{TL} and A_{TL} (see middle and right-hand panels of Fig. 1). Particularly interesting is the oscillatory structure of the fully relativistic result for A_{TL} . This characteristic is preserved by the positive-energy projection method of eq. (3), but not by the method of asymptotic projection. Note that the dependence on the dynamical enhancement of the lower components is stronger for the $p_{1/2}$ R_{TL} response than for $p_{3/2}$, a feature that was first seen in RPWIA [18] and that persists in RDWIA. On the other hand, the asymptotic projection severely modifies A_{TL} for both orbitals. We notice that the A_{TL} calculated with the asymptotic projection approach are very similar to the ones obtained in [29], as it corresponds to what is called EMA approach in said reference. The difference of the results obtained with different gauges, on the other hand tends to be smaller in the fully relativistic approach than in any of the projected or asymptotically projected cases.

At low momentum the asymptotic approach lies close to the fully relativistic one and to the exact positive-energy projection method, but beyond $p_m \simeq 200$ MeV/c it gives completely different results. The oscillating trend of the A_{TL} calculated in RDWIA is confirmed by the data [22] and agrees qualitatively with previous calculations by Van Orden [22].

Let us discuss now in detail how the results compare to experimental data. First, in Table 1 we show the spectroscopic factors needed by the different approximations in order to fit the experimental cross sections.

As seen in Fig. 1, the cross-sections look similar at low-medium values of the missing momentum, $|p_m| \leq 300$ MeV/c, although the spectroscopic factors that scale the different curves may differ up to a $\sim 10\%$. In the high- p_m region, $|p_m| \geq 300$ MeV/c, the different approaches produce results that can be rather different. Note that the two fully relativistic calculations, J_{cc1} (solid line) and J_{cc2} (dotted line), fit better the high- p_m experimental data than the projected calculations.

R_{TL} is presented in the middle panels for the two orbits: $1p_{1/2}$ (fig. 1, top) and $1p_{3/2}$ (fig. 1, bottom). The curves are scaled with the spectroscopic factors signaled in Table 1. Differences among the calculations are clearly visible for this observable. In the case of the $1p_{1/2}$ shell, the fully relativistic calculation with the $cc2$ current (dotted line) fits better the

experimental data, while the response obtained with the $cc1$ current operator (solid line) is a little bit too high (in absolute value). The cross-section based on the asymptotic projection peaks at slightly smaller p_m values than the fully relativistic ones, resulting in a somewhat poorer fit to the data. Finally, for this shell the R_{TL} response obtained with J_{++} is very different from the previous ones. This indicates that the findings of ref. [18,19], namely that the R_{TL} for $j = l - 1/2$ spin-orbits partners shows a large effect of the negative energy components, are still valid in DWIA. Remarkably enough, the projected result clearly fails to reproduce the data in this shell, while the fully relativistic results obtained with the $cc2$ operator nicely fits the experimental data, both at low and high momentum.

In the case of the $j = l + 1/2$ spin-orbit partner $1p_{3/2}$ orbit (Fig. 1, bottom), we find that the overall look of the responses obtained with the four approaches are similar, although the cross-section obtained with the asymptotic current again has a *faster* dependence with p_m than shown by the data. The other three approaches fit almost equally well all the data but the one point at the maximum, that is overestimated by the $cc1$ and $cc2$ relativistic calculations, and also, but to a less extent, by the J_{++} one. However, this projected calculation underestimates the high- p_m data for R_{TL} .

Finally at the left part of figures 1 and 2 we show the results for A_{TL} for both orbits. This observable does not depend on the spectroscopic factors. In the case of the $1p_{1/2}$ shell (Fig. 1, top), one can observe that the two fully relativistic calculations fit nicely the experimental data. The projected calculation (dashed line) follows the same general trend as the fully relativistic ones, but is smaller than the relativistic results, thus can not fit the data at low momentum. As already seen for R_{TL} , the negative energy components clearly affect the asymmetry for the $j = l - 1/2$ partner, largely improving the agreement with the experiment. The case of the asymptotic projected calculation deserves special attention because of its different behaviour compared to the previous ones, particularly for high momentum values. At low momenta, this approach lies close to the other three calculations, and given the fact that there are only two experimental data in this region, it is difficult to conclude which approach agrees better with the experiment. However, the highest p_m data clearly lies far from the asymptotically projected result predictions, but agrees with the other three calculations. The experimental error bar should be reduced by a factor two or more to disentangle which calculation is favoured by the data in this high- p_m region.

A similar discussion to the one presented for R_{TL} , could be also applied to the $1p_{3/2}$ orbit (fig. 1, bottom): the difference between the two fully relativistic calculations $cc1$ and $cc2$ and the projected one J_{++} is rather small, only important near the maximum (in absolute value) of the asymmetry, where the experimental data has a large error bar. This point is well described by both fully relativistic results but not by J_{++} . Furthermore, the asymptotic calculation clearly fails to reproduce the experimental data for this shell, except for the point at around 150 MeV, where all the calculations predict very similar results anyway.

Everything put together, the data on A_{TL} and R_{TL} are a strong indication of the presence and crucial role played by dynamical effects of relativity affecting the lower components, in the description of electron-nucleus scattering reactions.

Other relativistic effects can be seen in Fig. 2, where we compare RDWIA results on A_{TL} (left panels) and R_{TL} (right panels) to nonrelativistic approaches at various levels. To minimize the differences we have used the $cc2$ current operator and nonrelativistic scattered

wave functions obtained from Dirac-equivalent Schrödinger equations [12]. This ensures that the nonrelativistic wave functions correspond to the upper components of the relativistic ones, containing in particular the Darwin term. For the nonrelativistic bound wave functions, we used the ones in [27]. In [27,28] new approximations to the on-shell relativistic one-body current operator were developed to take better account of relativistic kinematic effects in nonrelativistic calculations. In particular, the charge density contains a spin-orbit correction that affects R_{TL} [27]. In Fig. 2 we show by long dashed lines the results obtained with the “relativized current” and by dotted lines the results obtained with that relativized current when the spin-orbit correction term to the charge-density is neglected. One can see that the spin-orbit correction has a very large effect on R_{TL} and A_{TL} . Its omission causes large deviations from the relativized current results. Using the DWEEPY [33] code we have obtained similar results to the dotted lines in Fig. 2.

The short dashed lines in Fig. 2 are results obtained with the relativistic current and 4-spinors constructed as in eq. (2) from the nonrelativistic bound and scattered wave functions. In this way, the relativistic kinematics are fully taken into account as well as the dynamical effect in the upper component, namely the effect of the Darwin term; only the dynamical enhancement of the lower components is missed. This is why these results (short-dashed lines) for A_{TL} and R_{TL} are much closer to the fully relativistic results shown by the solid lines. We see also that a large oscillation of A_{TL} can be recovered in the nonrelativistic approach. The much smaller oscillation of A_{TL} is a distinctive feature of the asymptotically projected calculation only, and it seems to be ruled out by the data. We also note that, while the effect of the dynamical enhancement of the lower components is larger in $p_{1/2}$ than in $p_{3/2}$ shells, the effects of relativistic kinematics are of the same order in both shells.

In conclusion, we have identified two types of relativistic effects on R_{TL} and A_{TL} . One is of kinematical origin, and has a large contribution from the spin-orbit correction to the charge density, and other is of dynamical origin. The latter is mainly due to the enhancement of the lower components and is stronger for $p_{1/2}$ than for the $p_{3/2}$ orbital. This is in addition to the dynamical effect on the upper component due to the Darwin term which is present in all the results given here, and that mostly affects the determination of spectroscopic factors [12]. It is encouraging that the data [22] agree so well with the predictions of the fully relativistic calculations and one anticipates being able to make even more stringent tests when a finer grid of high-precision data involving other nuclei become available in the range $200 \leq p_m \leq 400$ MeV/c.

This work was partially supported under Contracts No. 940183 (NATO Collaborative Research grant), #DE-FC01-94ER40818 (cooperative agreement with the US department of Energy D.O.E.), PB/95-0123, PB/95-0533-A, PB/95-1204, (DGICYT, Spain), PB/96-0604 (DGES, Spain), PR156/97 (Complutense University, Spain) and by the Junta de Andalucía (Spain).

REFERENCES

- [1] S. Frullani, J. Mougey, Adv. Nucl. Phys. 14 (1985). S. Boffi, C. Giusti, F.D. Pacati, Phys. Rep. 226 (1993) 1. S. Boffi, C. Giusti, F. Pacati, M. Radici in “*Electromagnetic Response of Atomic Nuclei*”, (Oxford-Clarendon Press, 1996). J.J. Kelly, Adv. Nucl. Phys. V 23 (1996) 77.
- [2] L. Lapikas, Nucl. Phys. **A553** (1993) 297c. E. Quint, Ph.D. Thesis, NIKHEF 1988.
- [3] I. Bobeldijk et al., Phys. Rev. Lett. 73 (1994) 2684.
- [4] K.I. Blomqvist et al., Phys. Lett. B 344 (1995) 85.
- [5] J. Ryckebush, D. Debruyne, W.N. Nespens, S. Janssen, nucl-th/9904011; V. Van der Sluys, J. Ryckebush and M. Waroquier, Phys. Rev. C **54** (1996) 1322.
- [6] J.E. Amaro, A.M. Lallena, J.A. Caballero, preprint nucl-th/9904030, Phys. Rev. C (in press).
- [7] V.R. Pandharipande, C.N. Papanicolas, J. Wambach, Phys. Rev. Lett. 53 (1984) 1133; Z.Y. Ma, J. Wambach, Phys. Lett. B 256 (1991) 1; C. Mahaux, R. Sartor, Adv. Nucl. Phys. 20 (1991) 1.
- [8] H. Mütter, W.H. Dickhoff, Phys. Rev. C 49 (1994) R17.
- [9] L. Chinitz *et al.*, Phys. Rev. Lett. **67** (1991) 568.
- [10] A. Picklesimer, J.W. Van Orden, Phys. Rev. C **35** (1987) 266; *ibidem* **40** (1989) 290.
- [11] J.M. Udías, P. Sarriguren, E. Moya de Guerra, E. Garrido, J.A. Caballero, Phys. Rev. **C48** (1993) 2731
- [12] J.M. Udías, P. Sarriguren, E. Moya de Guerra, E. Garrido, J.A. Caballero, Phys. Rev. **C51** (1995) 3246.
- [13] J.P. McDermott, Phys. Rev. Lett. 65 (1990) 1991; Y. Jin, D.S. Onley, L.E. Wright, Phys. Rev. C 45 (1992) 1311.
- [14] J.M. Udías, P. Sarriguren, E. Moya de Guerra, J.A. Caballero, Phys. Rev. **C51** (1996) R1488.
- [15] T. de Forest, Nucl. Phys. A 392 (1983) 232.
- [16] B.D. Serot, J.D. Walecka, Adv. Nucl. Phys. 16 (1986) 1.
- [17] E.D. Cooper, S. Hama, B.C. Clark, R.L. Mercer, Phys. Rev. C 47 (1993) 297.
- [18] J.A. Caballero, T.W. Donnelly, E. Moya de Guerra, J.M. Udías, Nucl. Phys. **A632** (1998) 323.
- [19] J.A. Caballero, T.W. Donnelly, E. Moya de Guerra, J.M. Udías, Nucl. Phys. **A643** (1998) 189.
- [20] S. Gilad, W. Bertozzi, Z.-L. Zhou, Nucl. Phys. **A631** (1998) 276c; E. Hummel, J.A. Tjon, Phys. Rev. **C49** (1994) 21; J.E. Ducret *et al.*, Phys. Rev. C **49** (1994) 1783.
- [21] G.M. Spaltro *et al.*, Phys. Rev. **C48** (1993) 2385. H.J. Bulten, Ph.D. thesis, University of Utrecht, 1992.
- [22] J. Gao, Ph.D. Thesis, Massachusetts Institute of Technology (1999). T Saha *et al.* TJNAF proposal 89-003 (1989).
- [23] M.M. Sharma, M.A. Nagarajan, P. Ring; Phys. Lett. B 312 (1993) 377.
- [24] C.J. Horowitz, D.P. Murdock, B.D. Serot in “*Computational Nuclear Physics*”, ed. K. Langanke, J.A. Maruhn and S.E. Koonin (Springer, Berlin 1991).
- [25] G.A. Lalazissis, J. König, P. Ring, Phys. Rev. C **55** (1997) 540.
- [26] M. Leuschner *et al.*, Phys. Rev. C **49** (1994) 955.
- [27] J.E. Amaro *et al.*, Nucl. Phys. **A602** (1996) 263; J.E. Amaro, J.A. Caballero, T.W.

- Donnelly, E. Moya de Guerra, *ibid.* **A611** (1996) 163; J.E. Amaro, T.W. Donnelly, *Ann. Phys.* **263** (1998) 56; *Nucl. Phys.* **A646** (1999) 187.
- [28] S. Jeschonnek and T.W. Donnelly, *Phys. Rev. C* **57**, 2439 (1998).
- [29] J.J. Kelly, *Phys. Rev. C* **56** (1997) 2672; nucl-th/9905024.
- [30] S. Boffi, C. Giusti, F.D. Pacati, F. Cannata, *Nuovo Cimento* **98**, 291 (1987).
- [31] Y. Jin, D.S. Onley, *Phys. Rev. C* **50**, 377 (1994).
- [32] M. Hedayati-Poor, J.I. Johansson, H.S. Sherif, *Phys. Rev. C* 51 (1995) 2044; *Nucl. Phys.* **A593** (1995) 377; J.I. Johansson, H.S. Sherif, G.M. Lotz, *ibidem* **A605** (1996) 517.
- [33] C. Giusti, F. Pacati, *Nucl. Phys.* **A473** (1987) 717; *ibid.* **A336** (1980) 427.

TABLES

Shell	CC1	CC2	Proj.	As. Proj.
$1p_{1/2}$	0.72	0.77	0.83	0.77
$1p_{3/2}$	0.70	0.76	0.84	0.77

TABLE I. Spectroscopic factors needed to fit experimental cross sections. The following nomenclature is used, CC1 and CC2: fully relativistic calculations with both current operators and Coulomb gauge. Proj.: relativistic calculations projection the wave functions over positive energy states. As. proj.: same as previous case but using the asymptotic values of the momenta. For the $p_{3/2}$ shell we took into account the small contribution from the near lying $5/2^+$ and $1/2^+$ states known from the low-p data [26].

FIGURES

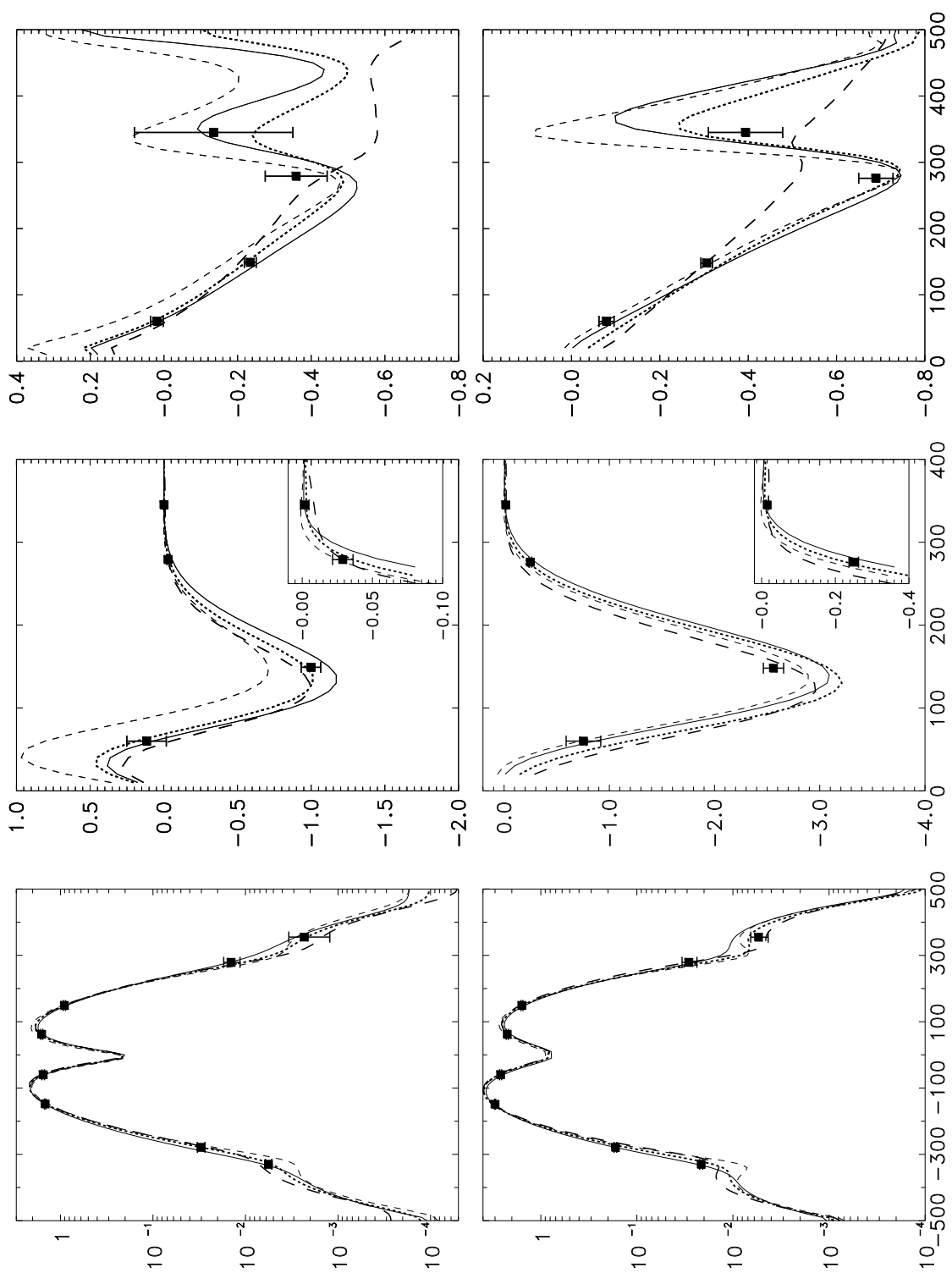


FIG. 1. Cross section in nb/MeV (left), R_{TL} in fm³ (middle) and A_{TL} (right) for proton knockout from ¹⁶O for the $1p_{1/2}$ (upper panel) and $1p_{3/2}$ (lower panel) orbits, versus missing momentum p_m in MeV/c. Results shown correspond to a fully relativistic calculation using the Coulomb gauge and the current operators: $cc1$ (solid line) and $cc2$ (dotted line). Also shown are the results after projecting the bound and scattered proton wave functions over positive-energy states (dashed line) and using the asymptotic momenta (long-dashed line).

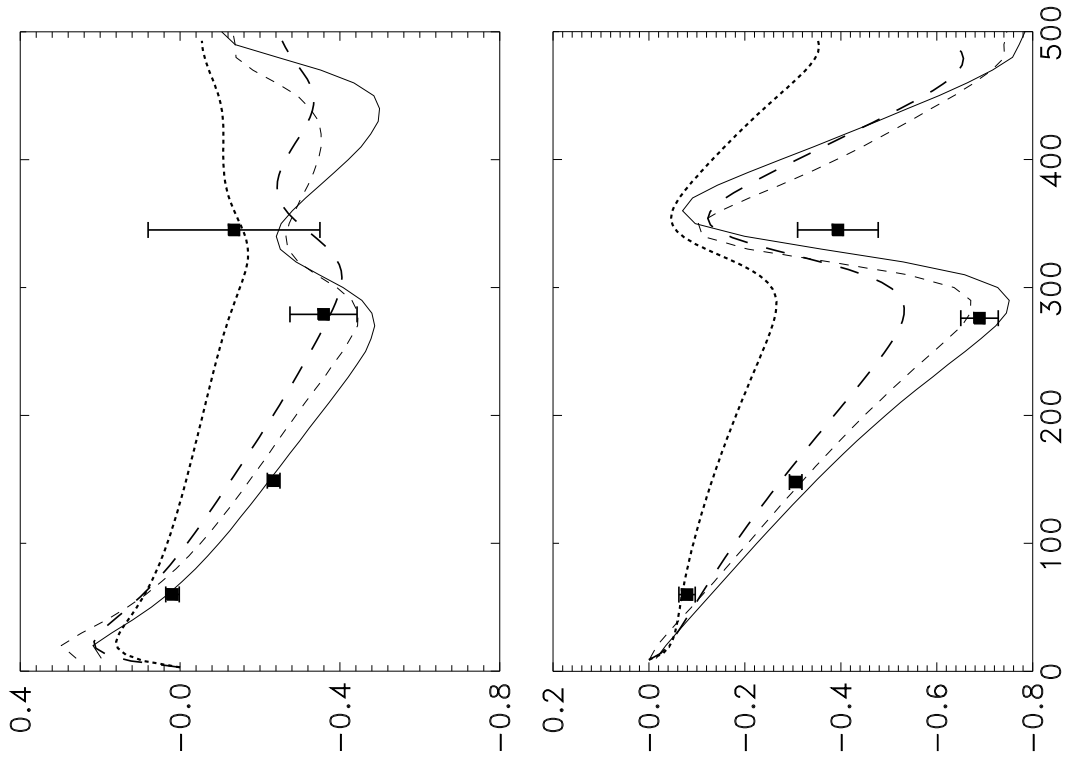
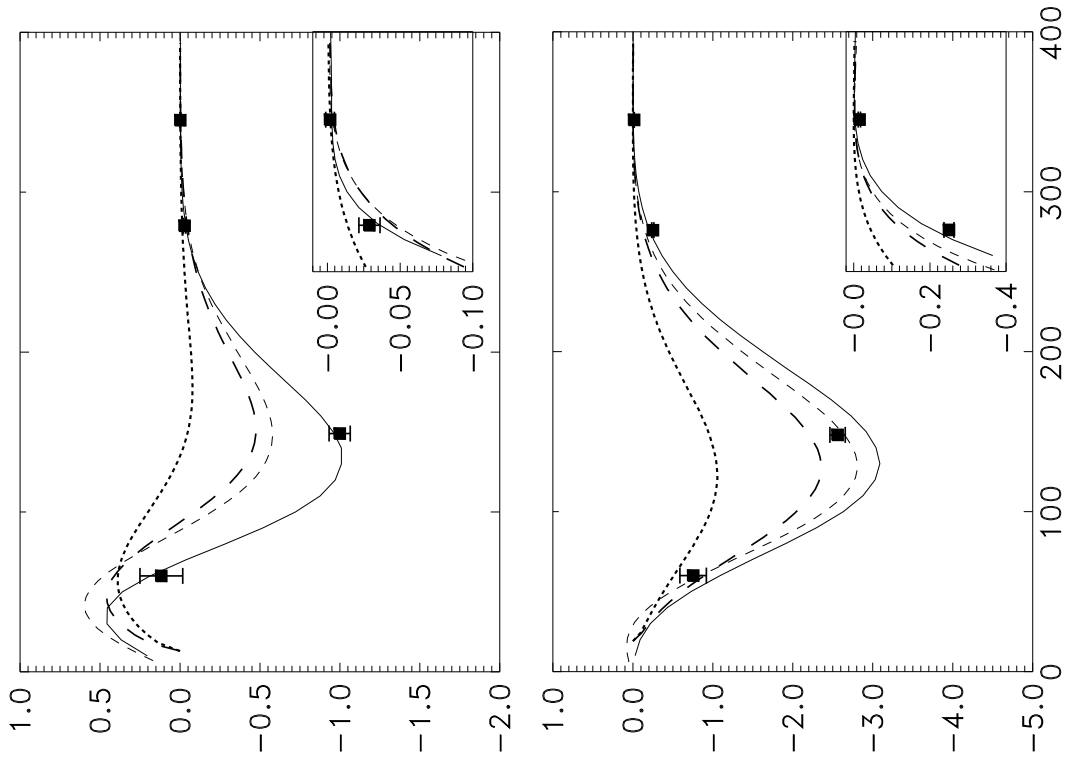


FIG. 2. R_{TL} (right panels) and A_{TL} asymmetries (left panels) for proton knockout from ^{16}O for the $1p_{1/2}$ (top panels) and $1p_{3/2}$ (bottom panels) orbits. Results shown correspond to a fully relativistic calculation using the Coulomb gauge and the current operator $cc2$ (solid line), a calculation performed by projecting the bound and scattered proton wave functions over positive-energy states (dashed line) and two nonrelativistic calculations with (long-dashed) and without (dotted) the spin-orbit correction term in the charge density operator (see text for details).